



Trap-assisted tunneling current of ultrathin InAlN/GaN HEMTs on Si (1 1 1) substrate



Jingxian Liang^{a,b}, Longkun Lai^a, Zhaokun Zhou^b, Jing Zhang^b, Jie Zhang^a, Jin Xu^a, Yipeng Zhang^b, Xinyu Liu^a, Weijun Luo^{a,*}

^a Institute of Microelectronics of Chinese Academy of Sciences, University of Chinese Academy of Sciences, China

^b North China University of Technology, China

ARTICLE INFO

Keywords:

InAlN/GaN
N₂ plasma interface passivation
Trap-assisted tunneling (TAT)
XPS

ABSTRACT

In this paper, the reverse gate leakage current mechanism of ultrathin InAlN/GaN high-electron mobility transistors on Si (1 1 1) substrate which treated with and without surface treatment process is systematically investigated. Current-voltage (*I*-*V*) measurement in temperature range from 273 K to 473 K and capacitance-voltage (*C*-*V*) measurement under 300 K are used to analyze the main leakage mechanism. For the whole reverse bias region (-30 V to 0 V), the best reasonable fitting calculation results correspond to the experimental values is based on trap-assisted tunneling (TAT) current mechanism, which indicates the dominant reverse leakage current of the ultrathin InAlN/GaN HEMTs device is derived from TAT current. N₂ plasma surface treatment method is proposed to optimize the interface of the Schottky contact, which is an important way to reduce the reverse leakage current examined by the extracted values of trap energy levels (φ_t) and thermal activation energy (E_a) as well as XPS results. Further, for high reverse bias condition, electric field saturation across the barrier layer is not sufficient to support the slow rise trend of the TAT current, a modified electric field model was proposed to accurately explain this phenomenon.

1. introduction

Lattice matched InAlN/GaN high-electron-mobility transistors (HEMTs) are excellent candidates for electronic applications owing to its promising electronic properties and polarization effects [1]. On the other hand, the growth of InAlN/GaN epitaxial layer on Si substrate (among the choices of SiC, sapphire, Si, and GaN substrate) is very suitable for commercialization for its low cost and superior scalability in wafer size [2]. However, large reverse-bias gate leakage remains a pressing issue which plague the use of high-voltage application. Analyzing and reducing the reverse gate leakage current in InAlN/GaN HEMTs is essential to their incorporation into circuits and systems.

For HEMT devices, the 2DEG in the channel is controlled by the gate Schottky diode. Since lattice-matched InAlN is considered to be a strain-free barrier layer on GaN. Therefore, even in the absence of piezoelectric polarization, its higher spontaneous polarization coefficient produces a higher 2DEG concentration. Moreover, in the case of the surface potential of the InAlN barrier is located approx. 0.4 eV below the conduction band even without passivation. A high current density of 1.1 A/mm can still be obtained in planar 5 nm barrier devices [3].

This advantages make it possible to allow the InAlN barrier to be thinner without compromising 2DEG concentration. Furthermore, high 2DEG concentration make it necessary to turn off the device with large negative bias voltage [4]. Thus the gate leakage becomes significant in deciding the standby power dissipation and the reliability of the device. The experimental value of the gate leakage current in the InAlN/GaN HEMTs was observed to be much larger than the theoretical value of thermionic emission. (TE) [5]. Therefore, further analysis of gate leakage mechanism is needed. To date, there are only a few reports on the gate leakage mechanisms for ultrathin InAlN/GaN HEMTs. Satyaki Ganguly et al illustrated the dominant conduction mechanism of InAlN/GaN HEMTs on SiC substrate in low to medium reverse bias voltages is Frenkel-Polle (FP), while Fowler-Nordheim (FN) tunneling is observed at high reverse bias voltages [5]. S. Turuvekere et al analyzed the mechanism on sapphire substrates suggested Trap Assisted Tunneling (TAT) where traps are involved in electron capture and emission, which results in the leakage current passing through Schottky barrier [4]. Junji Kotani et al proposed the leakage current mechanism on GaN substrate is that a dislocation-related Frenkel-polle (FP) thermal emission in the low bias region, and demonstrated that the reduction of

* Corresponding author.

E-mail address: luoweijun@ime.ac.cn (W. Luo).

dislocation density is effective in reducing leakage current [6]. In addition, so far, no paper on analysis of gate leakage mechanism in ultrathin InAlN/GaN on Si (1 1 1) substrate. The leakage current mechanism of AlGaN/GaN on Si (1 1 1) substrate reported by Y. Li et al was considered, the dominant leakage current is the FP emission at low to medium reverse bias region, and Trap Assisted Tunneling (TAT) is dominated in the higher reverse bias region [7,8]. Compared to other substrate materials, the large lattice mismatch exist between InAlN/GaN epitaxial layer and Si substrate. S. J. Rosner et al also reported that defects in the depletion buffer layer may participate in the conduction [9]. Thus, Although these reports [5–8] have analyzed the mechanism in InAlN/GaN of the reverse leakage current, they are restricted either to a small bias voltage ($-10 \text{ V} < V_R < 0 \text{ V}$) and/or substrate on SiC, sapphire, GaN. So far, there are no reports on the study of gate leakage mechanism in ultrathin InAlN/GaN on Si (1 1 1) substrate.

In this paper, the mechanism of reverse leakage current in a wide range of reverse bias ($-30 \text{ V} < V_R < 0 \text{ V}$) and temperature (273 K–473 K) has been analyzed in detail. An optimized N₂ plasma surface treatment of InAlN/GaN HEMTs Schottky contact fabrication was proposed, and revealed by XPS analysis. For high bias condition, considering the influence of buffer layer for the first time, a modified electric field model was proposed to accurately explain the slowly rising trend of the reverse leakage. To the best of our knowledge, it is the first time the gate leakage mechanism in ultrathin InAlN/GaN on Si (1 1 1) substrate has been reported.

This paper is arranged as follows. In Section II, the fabrication process and the device characterization techniques of InAlN/GaN HEMTs are described. Temperature dependence of gate reverse current-gate voltage (J_R - V_R) characteristics of InAlN/GaN in different reverse bias voltage are presented and compared in Section III. Finally, the conclusions are drawn in Section IV.

2. experiment

The epitaxial layers of InAlN/GaN HEMTs used in this paper were grown on a 4-in high-resistivity (~11 Kohm·cm) Si (1 1 1) substrate by Metal Organic Chemical Vapor Deposition (MOCVD). The epitaxial layers includes GaN buffer layer of 1-μm thickness, and InAlN barrier layer of 7-nm thickness with In mole fraction of 17%. The InAlN/GaN HEMTs fabrication procedures consists of Ti/Al/Ni/Au ohmic contact metallization, followed by annealing at 870 °C for 30 s in N₂. Nitrogen ion implanting was used for isolation. F-based plasma etch the top Si₃N₄ passivation down to the InAlN layer. Subsequently, the wafer was divided into two parts. Before the formation of Ni/Au Schottky gate, we treated the gate recessed area with different methods: Sample (A), the N₂ (20 sccm) plasma surface treatment was performed with an RF power of 15 W and a pressure of 3 Pa for a time of 3 min. While sample (B) did not have a N₂ plasma surface treatment. Followed by evaporation, the gate length, gate width, and source-to-drain spacing are 0.25 μm, 60 μm, and 3.5 μm, respectively. A 2DEG electrons concentrations of $3.18 \times 10^{13} \text{ cm}^{-2}$, electron mobility of 870 cm²/V·s and sheet resistance of 389.8 ohm/sq were obtained by Hall-effect measurements at room temperature. The GaN (0 0 2) and GaN (1 0 2) XRD FWHM values are 660arcsec and 1500arcsec, respectively. I - V characterization was measured in the dark using Agilent BP 1500 in the temperature range of 273 K–473 K, with a step increment of 50 K, and capacitance-voltage (C-V) was carried out at room temperature.

3. results and discussion

The reverse gate leakage current density (J_R)-voltage (V_R) characteristics at different temperatures are shown in Fig. 1 and Table 1. It is observed that the reverse gate leakage current of the device increase as the temperature and the reverse bias voltage increases. As can be seen from the Table 1, the leakage current density of sample (B) is about two to three times larger than that of the current density of sample (A)

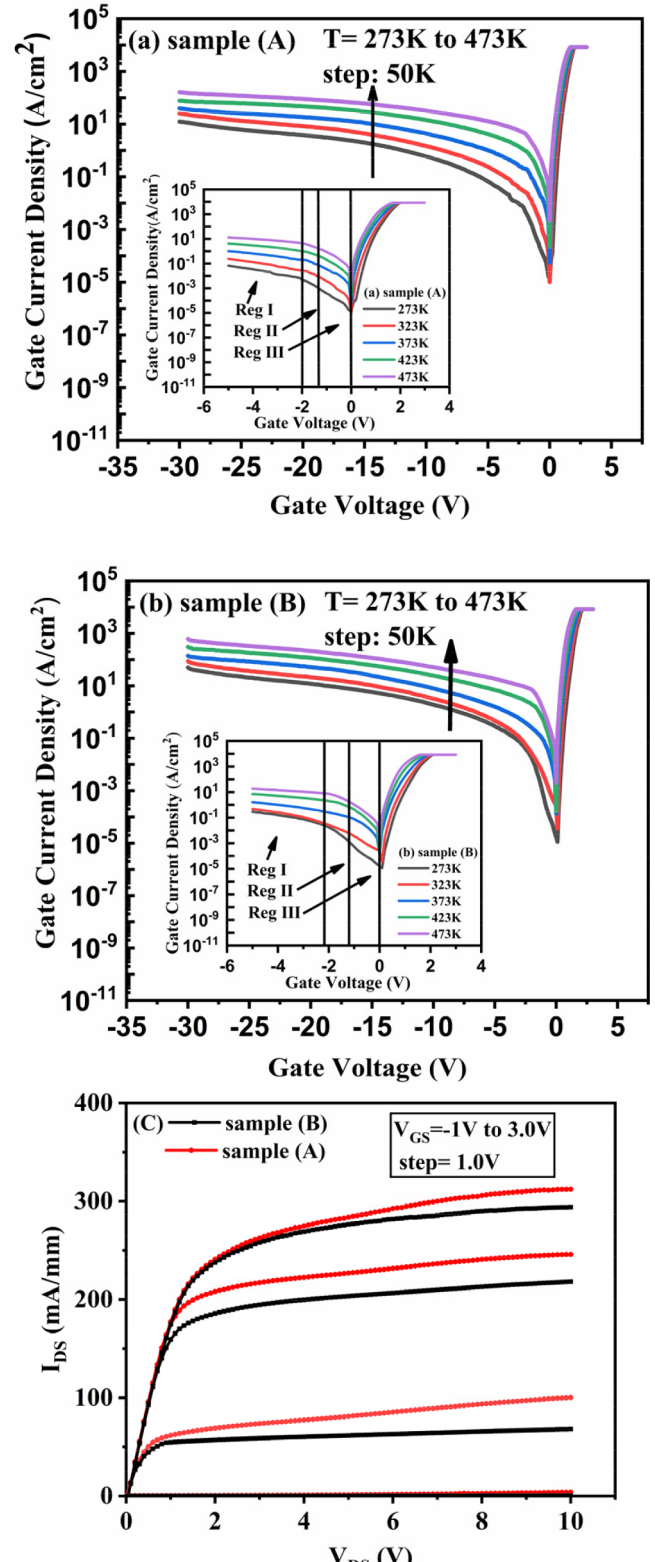


Fig. 1. Reverse gate current density-gate voltage characteristics of two samples at different temperatures. Inset: Division of reverse leakage current under different bias voltages. Plot of the I_{DS} - V_{DS} characteristics.

under the same reverse bias voltage. Correspondingly, under a certain bias V_{GS} , the I_{DS} of sample (A) is nearly the same as sample (B). In order to investigate the reverse gate leakage mechanism of the ultrathin Si (1 1 1) based InAlN/GaN HEMTs, the Schottky leakage mechanism

Table 1
Current density of sample (a) and sample (b) at different bias.

Voltage (V)	Sample (A) JR (A/cm ²)	Sample (B) JR (A/cm ²)
-30	25.094	88.139
-25	13.350	37.132
-20	8.349	21.223
-15	1.479	3.219
-10	0.242	0.467
-2.5	0.038	0.057
-1.5	0.002	0.004

under low, medium, high reverse bias voltage were analyzed, respectively.

3.1. Leakage current mechanisms at low to middle reverse bias voltage

As shown in Fig. 1, at low reverse bias (sample (A): in Reg III, $-0.7 \text{ V} < V_R < 0 \text{ V}$, sample (B) : in Reg III, $-0.6 \text{ V} < V_R < 0 \text{ V}$) and at middle reverse bias (sample (A): in Reg II, $-2.0 \text{ V} < V_R < -0.7 \text{ V}$ sample (B): in Reg II, $-2.3 \text{ V} < V_R < -0.6 \text{ V}$), a clearly increase in the reverse leakage current with increase of temperature is observed, which is same with the other reported results [7,8]. Mechanisms related to temperature, such as Thermionic emission (TE), Poole-Frenkel emission (PF) and trap-assisted tunneling (TAT), will be focused to analyze the reverse leakage current mechanism of the proposed InAlN/GaN HEMTs samples.

3.1.1. Thermionic emission current (TE)

Considering the leakage current in ultrathin Si (1 1 1) based InAlN/GaN HEMTs, for thermionic emission, the carriers absorb the thermal energy and then emit over the potential barrier at the M-S interface. The J_R-V_R characteristics of thermionic emission is described by the expression [7]

$$J_{TE} = A * T^2 \exp \left[-\frac{q}{K_B T} \left(\phi_B - \sqrt{\frac{qE}{4\pi\epsilon_s(h)\epsilon_0}} \right) \right] \quad (1)$$

In Eq. (1), A^* is the effective Richardson's constant, T , q , K_B , and ϵ_0 are the temperature, the electron charge, the Boltzmann's constant, the vacuum permittivity, respectively. $\epsilon_s(h)$ is the high-frequency (optical) dielectric constant of $\text{In}_{0.17}\text{Al}_{0.83}\text{N}$. $q\phi_B$ is the Schottky barrier height and E is the electric field at the M-S interface. Eq. (1) can be rearranged as

$$\ln(J_{TE}/T^2) = K_{TE}(T) \sqrt{E} + C_{TE}(T) \quad (2)$$

where

$$K_{TE}(T) = \frac{q}{2K_B T} \sqrt{\frac{q}{\pi\epsilon_s(h)\epsilon_0}} \quad (3)$$

$$C_{TE}(T) = -\frac{q\phi_B}{K_B T} + \ln(A^*) \quad (4)$$

To estimate the near-surface electric field E underneath the Schottky contact metal, a high frequency (1 MHz) C-V scan is used to determine the 2DEG density at the InAlN/GaN interface as a function of reverse bias. And, the diameter of the ring Schottky diodes is 133 μm. The C-V curves are shown in Fig. 2. From the C-V curves, the extracted V_{Th} of sample (A) and sample (B) are -2.0 V and -2.3 V , respectively. The threshold voltage of sample (A) could be positively shifted with the reduction of the interface state charge by the N₂ plasma treatment. And from the C-V curves, the accumulation area capacitance of sample (A) is larger than that of sample (B). Since N₂ plasma surface treatment is a physical bombarding process, it may slightly thinning down the thickness of the barrier layer, resulting in an increase in the capacitance of

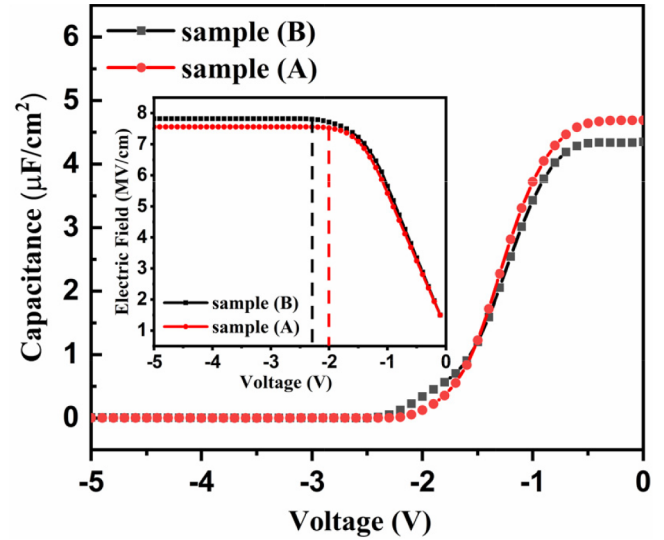


Fig. 2. Plot of the Capacitance-Voltage characteristics. Insert: the electric field as a function of the voltage for the InAlN/GaN HEMTs.

accumulation area. The $n_{2\text{DEG}}$ can be calculated by integration of the C-V curve from pinch-off voltage to 0 V. The electric field (E) across the barrier can be described by the expression [10]

$$E = \frac{q(\sigma_p - n_{2\text{DEG}})}{\epsilon_0 \epsilon_r} \quad \text{For } V_R \geq V_{Th} \quad (5)$$

where σ_p is the fixed polarization charge at hetero-interface, which is estimated to be $2.35 \times 10^{13} \text{ cm}^{-2}$ [5], $\epsilon_r = 10.25$ is the relative dielectric constant, n_0 is $n_{2\text{DEG}}$ at zero-bias voltage. A plot of electric field as a function of the gate voltage are shown in Inset of Fig. 2. As described in Eq. (5), the electric field is related to the fixed polarization and $n_{2\text{DEG}}$. The electric field is in proportional to the changing rate of the capacitance. The capacitance near the zero-bias of the InAlN/GaN HEMTs with ultrathin barrier layer is about $4.6 \mu\text{F}/\text{cm}^2$ (sample (A)), which is extremely larger than that of $0.7 \mu\text{F}/\text{cm}^2$ [5]. Therefore the electric field near the threshold voltage obtained by the C-V integration is $7.5 \text{ MV}/\text{cm}$. The electric field will be used to explain the leakage mechanism in subsequent analysis.

The $\ln(J_{TE}/T^2)$ vs. $E^{0.5}$ characteristics of the two samples at various temperatures are shown in Fig. 3(a), (b). According to the Eq. (2), the $\ln(J_{TE}/T^2)$ and $E^{0.5}$ should fulfill the linear relationship with the slope K_{TE} . Fig. 3(a) and (b) shows the measured data fit well with straight lines at various temperatures, respectively. However, the extracted K_{TE} of sample (A) versus $1000/T$ from the $\ln(J_{TE}/T^2)$ vs. $E^{0.5}$ measurement is much large than theoretical value. Besides, the extracted K_{TE} of sample (B) is not corresponding to the Eq. (3). Therefore, the thermionic emission is not the principal leakage current at low reverse bias voltage.

3.1.2. Poole-Frenkel emission current (PF)

For the Poole-Frenkel (PF) emission mechanism, the carrier transport occurs through a trap state to the conductive continuum states with the assistance of electric field. PF emission current is generally given by [7].

$$J_{PF} = qn_0 u E \exp \left[-\frac{q}{K_B T} \left(\varphi_t - \sqrt{\frac{qE}{\pi\epsilon_s(h)\epsilon_0}} \right) \right] \quad (6)$$

In Eq. (6), u is the electron mobility of InAlN/GaN HEMTs, $q\varphi_t$ is the effective barrier height for electron emission from a trapped state. The Eq. (6) can be rearranged as

$$\ln(J_{PF}/E) = K_{PF}(T) \sqrt{E} + C_{PF}(T) \quad (7)$$

where

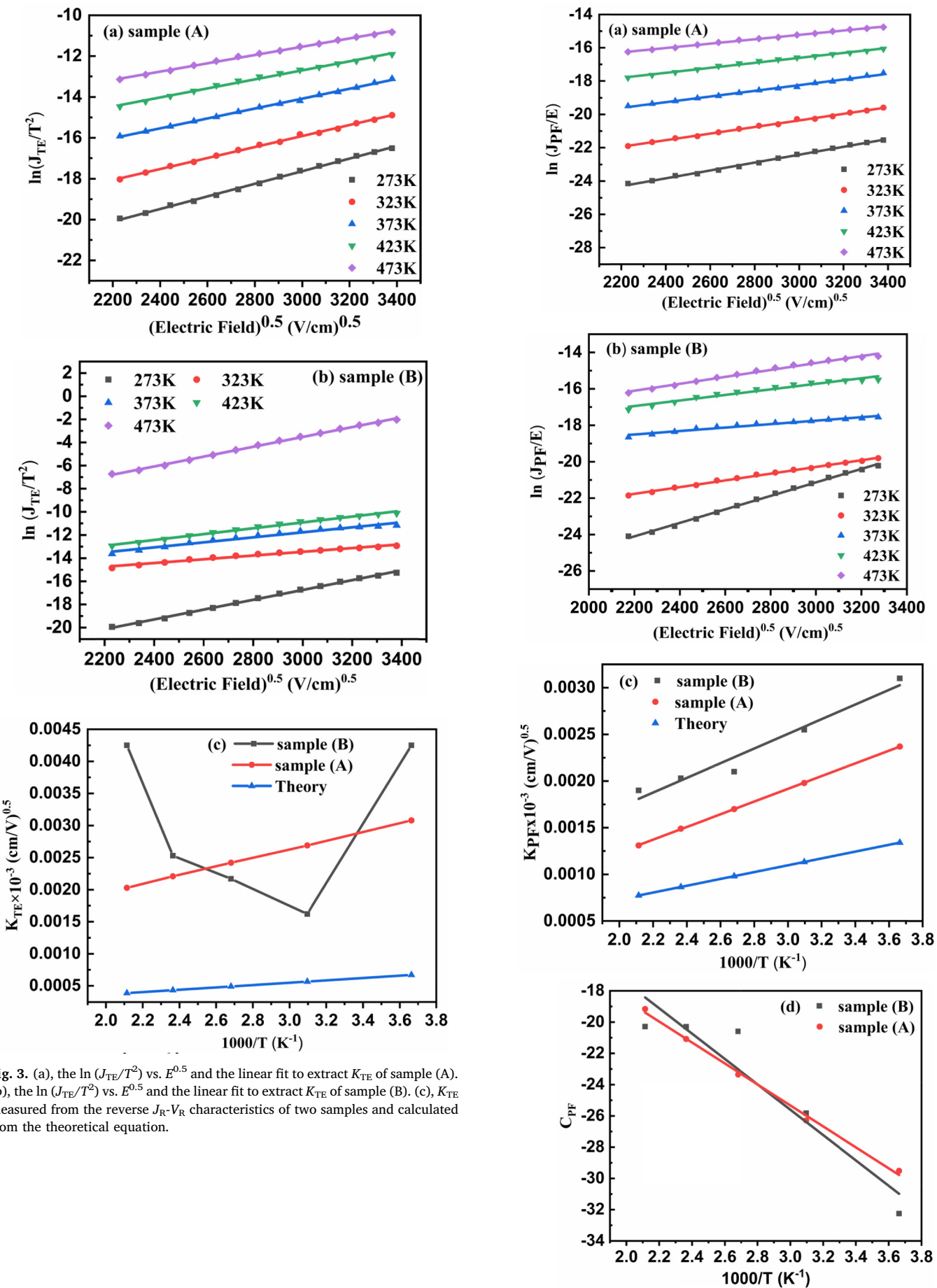


Fig. 3. (a), the $\ln(J_{TE}/T^2)$ vs. $E^{0.5}$ and the linear fit to extract K_{TE} of sample (A). (b), the $\ln(J_{TE}/T^2)$ vs. $E^{0.5}$ and the linear fit to extract K_{TE} of sample (B). (c), K_{TE} measured from the reverse J_R - V_R characteristics of two samples and calculated from the theoretical equation.

Fig. 4. (a), the $\ln(J_{PF}/E)$ vs. $E^{0.5}$ and the linear fit to extract K_{PF} of sample (A). (b), the $\ln(J_{PF}/E)$ vs. $E^{0.5}$ and the linear fit to extract K_{PF} of sample (B). (c), (d), K_{PF} and C_{PF} measured from the reverse J_R - V_R characteristics of two samples and calculated from the theoretical equation.

$$K_{PF}(T) = \frac{q}{K_B T} \sqrt{\frac{q}{\pi \epsilon_s(h) \epsilon_0}} \quad (8)$$

$$C_{PF}(T) = \frac{q \phi_t}{K_B T} + \ln(qn_0 u) \quad (9)$$

Eq. (7) suggests that the plot of $\ln(J_{PF}/E)$ versus $E^{0.5}$ should yield a straight line if the leakage current is caused by PF emission. This experimental measured curves of $\ln(J_{PF}/E)$ vs. $E^{0.5}$ in the temperature range of 273 K–473 K are shown in Fig. 4(a), (b). It is distinct that the measured $\ln(J_{PF}/E)$ of the two samples can be well fitted with $E^{0.5}$ at different temperature. Further, the K_{PF} extracted from measured curves at different temperature are compared to the calculated theoretical value. As shown in Fig. 4(c), the extracted K_{PF} of sample (A) and sample (B) are fitted well with straight lines at various temperature, respectively. Though the values of K_{PF} deviate from the theoretical values by a factor of 1.7–2.3, the values of ϵ_s of sample (A) and sample (B) are extracted from the slope of the fitting curve of K_{PF} with $T/1000$, which are 1.67 and 1.26, respectively. Since $\epsilon_{AlN} = 4.77$, $\epsilon_{InN} = 8.4$, the proposed ϵ_s of InAlN should be between ϵ_{AlN} and ϵ_{InN} . But the extracted values of ϵ_s are much smaller than the theoretical value of 6.2 [5]. So the PF mechanism shouldn't be the dominant mechanism of the reverse leakage current in the text.

The values of C_{PF} were extracted from Fig. 4(a) and (b), and plot a curve as a function of $1000/T$. As shown in Fig. 4(d), the C_{PF} values fits a straight line as a function of $1000/T$ and the extracted values $q\phi_t$ of the sample (A) and the sample (B) are 0.48 eV and 0.65 eV, which are similar to that of 0.48 eV in [5] and 0.54 eV [4]. However, the extracted values of ϵ_s is unreasonable as mentioned above. Therefore, the reverse leakage current is unlikely dominated by Poole-Frenkel (PF) emission mechanism at low to middle reverse bias. This points to some other dominant mechanism under low to middle reverse bias.

3.1.3. Trap-assisted tunneling current (TAT)

For the trap-assisted tunneling mechanism, the electron tunnels from gate metal to drain metal through the traps existed in barrier layer at reverse bias voltage. The tunneling current density J_{TAT} is given by [11].

$$J_{TAT} \propto \exp\left(\frac{-8\pi\sqrt{2qm_n^*}}{3hE}\phi_t^{3/2}\right) \quad (10)$$

where $q\phi_t$ is the trap energy level, m_n^* is the conduction band effective mass in semiconductor, h is the Planck's constant.

Fig. 5 shows this experimentally measured curve of $\ln(J_{TAT})$ vs. $1/E$ in the temperature range of 273 K–473 K. It can be seen that there is a transition in the middle and low bias. The electric field E corresponding to the transition is 4.97 MV/cm calculated from Fig. 2. This transition value of electric field is consistent with that of D. Mahaveer Sathaiya et al reported in [12], which explained that trap-assisted tunneling through a trapezoidal barrier at low fields (< 5 MV/cm) and through a triangular barrier at high fields (> 5 MV/cm). So, the low to middle bias are divided into two regions by the transition, corresponding to the Reg II and Reg III as shown in Fig. 1. The gate bias voltage of Reg II and Reg III are $-2.0 \text{ V} < V_R < -0.7 \text{ V}$ and $-0.7 \text{ V} < V_R < 0 \text{ V}$ for sample (A), while $-2.3 \text{ V} < V_R < -0.6 \text{ V}$ and $-0.6 \text{ V} < V_R < 0 \text{ V}$ for sample (B), respectively. Further, Fig. 5 (a), (b) shows the measured curve of $\ln(J_{TAT})$ vs. $1/E$ in the temperature range of 273 K–473 K. It is

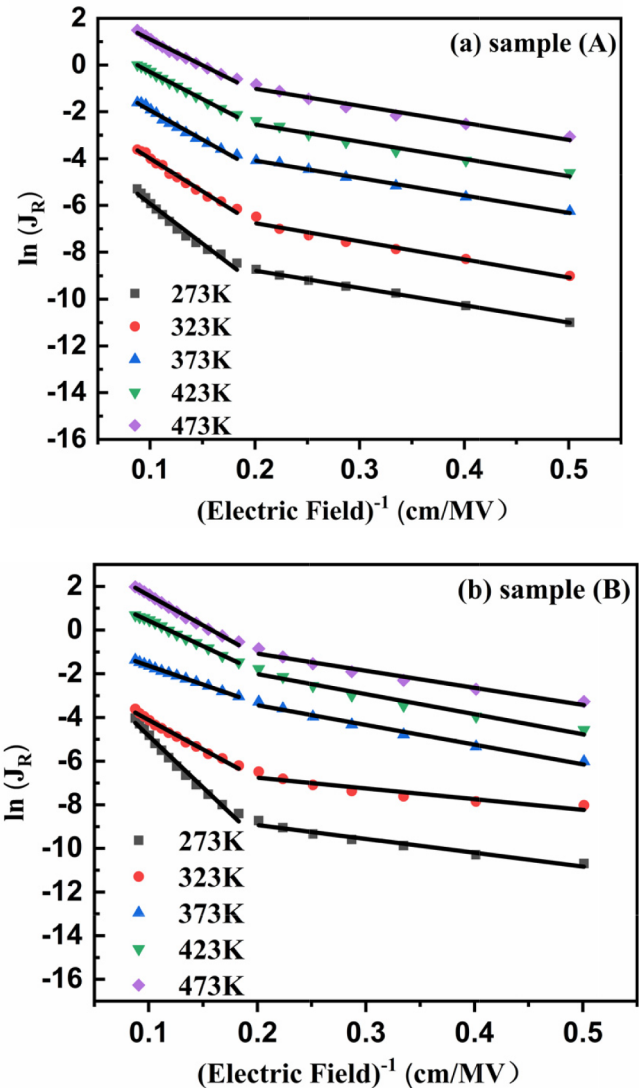


Fig. 5. (a), (b), $\ln(J_R)$ vs. $1/E$ plot of sample (A) and sample (B), respectively.

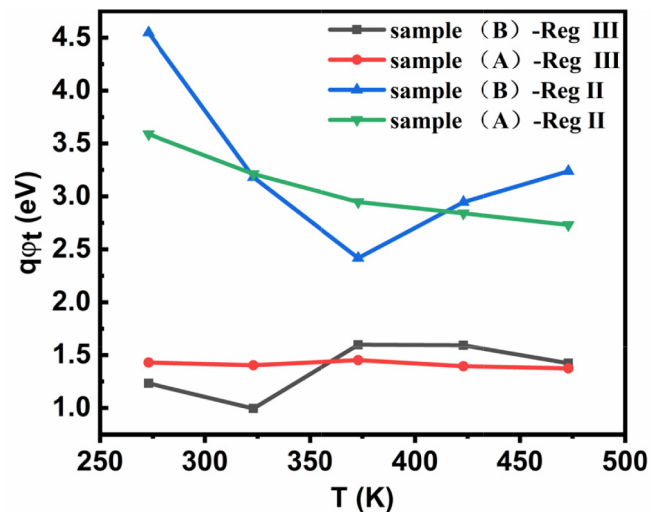


Fig. 6. The extracted $q\phi_t$ at different temperature of sample (A) and sample (B) under the Reg II and Reg III.

distinct that the measured $\ln(J_{\text{TAT}})$ of two samples can be well fitted with $1/E$ at different temperature in Reg II and Reg III. This confirms the dominant mechanism in low to middle reverse bias voltage is TAT. Furthermore, the trap state energy levels $q\varphi_t$, which is below the conduction band edge, can be extracted from the slope of the $\ln(J_{\text{TAT}})$ vs. $1/E$ curves using the effective mass of electron in InAlN as $0.4 m_e$ where m_e is the free electron mass [4]. For sample (A), the corresponding $q\varphi_t$ at different temperature of Reg II and Reg III are 2.7 eV – 3.5 eV and 1.37 eV – 1.42 eV, respectively. For sample (B), the corresponding $q\varphi_t$ at different temperature of Reg II and Reg III are 2.4 eV – 4.55 eV and 1.2 eV – 1.60 eV as shown in Fig. 6, respectively.

As shown in Fig. 6, $q\varphi_t$ decreases with the increase of temperature in Reg II, while changes little in Reg III. The reason is that forbidden band will slightly shrink as the temperature increases, thereby reducing the trap energy levels ($q\varphi_t$). And for sample (A) and sample (B), the extracted $q\varphi_t$ of Reg II is significantly larger than that of Reg III. This is also because when the electric field is less than 4.97 MV/cm, the electrons may tunnel through the trapezoidal barrier. As the reverse bias increases, when the electric field exceeds 4.97 MV/cm, the electrons may tunnel through the triangular barrier. The increase in reverse bias voltage causes the band to bend further, resulting in a decrease of the effective Schottky barrier height. The position of the trap state is reduced relative to the conduction band. Therefore, the extracted $q\varphi_t$ by Reg II is significantly larger than that of Reg III. In Reg III, for sample (A) and sample (B), the $q\varphi_t$ values of 1.37 eV – 1.42 eV and 1.2 eV – 1.60 eV are extracted at a low reverse bias voltage ($-0.7 \text{ V} < V_R < -0.1 \text{ V}$ corresponding to $1.9 \text{ MV/cm} < E < 5 \text{ MV/cm}$), which is lower than that of 1.7 eV – 2.3 eV at reverse bias ($-3.3 \text{ V} < V_R < -0.1 \text{ V}$ corresponding to $0.1 \text{ MV/cm} < E < 0.13 \text{ MV/cm}$) reported by Hui Liu et al [12]. Though the InAlN and AlGaN has different trap energy level, the main reason may be the big difference of electric fields between the two kinds of devices. Due to the ultrathin barrier layer, the electric field of InAlN in this work is about 7.5 MV/cm, which is obviously larger than that of 2.2 MV/cm of AlGaN sample in [13]. Meanwhile, the $q\varphi_t$ values of sample (A) and sample (B) at middle bias voltage (Reg II: $-2.0 \text{ V} < V_R < -0.7 \text{ V}$) are 2.7 eV – 3.5 eV and 2.4 eV – 4.55 eV, which are close to that of 2.87 eV – 3.32 eV reported by E. Suzuki et al [14]. So, it can be conclude that the TAT mechanism is consistent in the middle and low bias regions of the two samples. Besides, the extracted $q\varphi_t$ of both Reg II and Reg III for sample (B) is larger than that of sample (A). This could mainly be related to the N_2 plasma surface treatment, which might change the position of the trap states level $q\varphi_t$, thus affecting reverse leakage current. This will be discussed later by using XPS measurement. Lee et al have also reported that N_2 surface treatment can reduce reverse leakage current [15].

3.2. Leakage current mechanisms at high reverse bias voltage

The results and discussions mentioned above indicate that the two samples are dominated by the TAT mechanism in the low to middle reverse bias. When the reverse gate bias voltage ($V_R < V_{\text{Th}}$) is further increased, the electric field across the barrier increases resulting in the thinning of the tunneling barrier. And, carriers can more easily to tunnel across the triangular barrier. Then the conduction mechanism in the high reverse bias is more likely to be characterized by the tunneling mechanism. Therefore, for PF and TE emission mechanism cannot exist under the high filed. Therewithal, Fowler-Nordheim Tunneling (FN), Two-dimensional Variable Rang Hopping (2D-VRH) mechanism and a thermally activated trap-assisted tunneling (TAT) process are considered to be probable mechanism. Satyaki Ganguly et al, reported the FN tunneling current is dominant in the high reverse bias Reg I [5]. Usually, the reverse leakage current of the FN tunneling keep the same when the temperature increases. However, as shown in Fig. 1 and Table 1, the reverse leakage is clearly increased with the rising of temperature. Thus, it is impossible to be a FN tunnel current. In addition, Hui Liu et al confirmed that the surface leakage is a main leakage

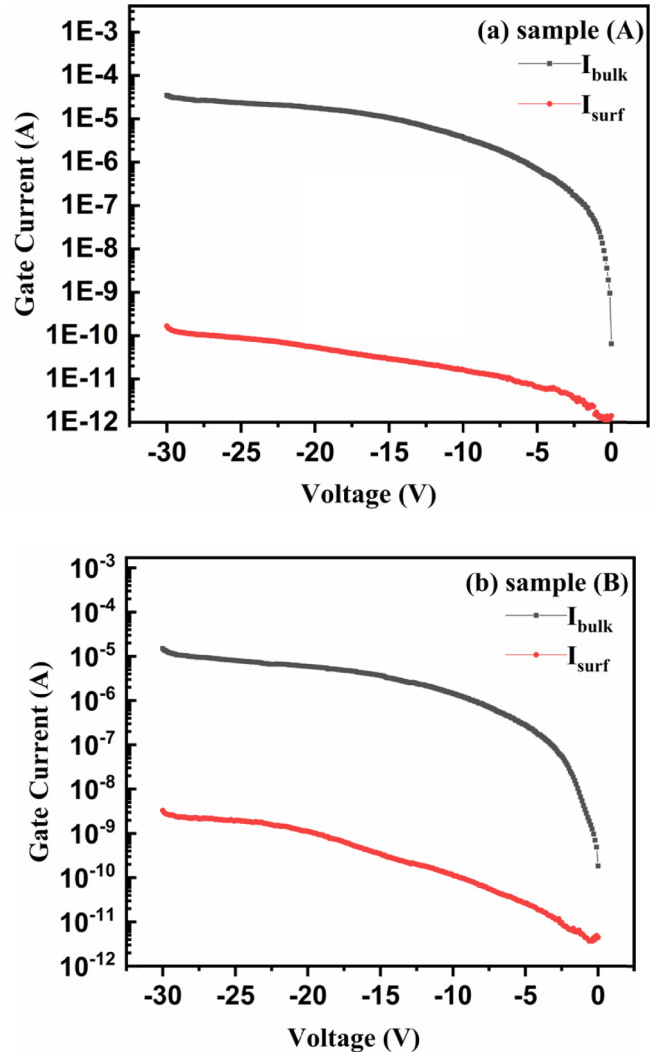


Fig. 7. Plots of reverse surface leakage current and bulk leakage current versus voltage at 323 K.

mechanism at high reverse bias voltage [13]. So, the surface leakage mechanism is also considered at high reverse bias voltage. By utilizing a dual-gate structure with gate pitch of $2.5 \mu\text{m}$ and gate width of $60 \mu\text{m}$, the reverse surface leakage current can be accurately assessed. Then, the relationship between the reverse surface leakage current I_{surf} and the bulk leakage current I_{bulk} versus the gate voltages of the samples (A) and (B) are shown in Fig. 7. It is clearly that the vertical bulk leakage is larger than the lateral surface leakage four to five orders of magnitude. Therefore, the leakage mechanism is unlikely to be surface leakage in the high field, it is more likely to be the thermally activated trap-assisted tunneling (TAT) mechanism.

In TAT mechanism under high reverse bias condition, electrons with an activation energy E_a are thermally activated to the trap states in barrier layer and tunneling through the barrier. E_a is the activation energy from the Fermi level to trap states. In high reverse bias, electric field is much larger than 4.9 MV/cm. So electron might tunnel through the triangular barrier, its effective tunneling barrier becomes thinner. As shown in the Reg I of Fig. 1, reverse leakage current density is increasing with the increase of temperature, suggesting a thermally activated process which can be described with the follow equation [7].

$$J_R \propto \exp\left(-\frac{E_a}{K_B T}\right) \quad (11)$$

where T is the temperature, J_R is the reverse saturation current density,

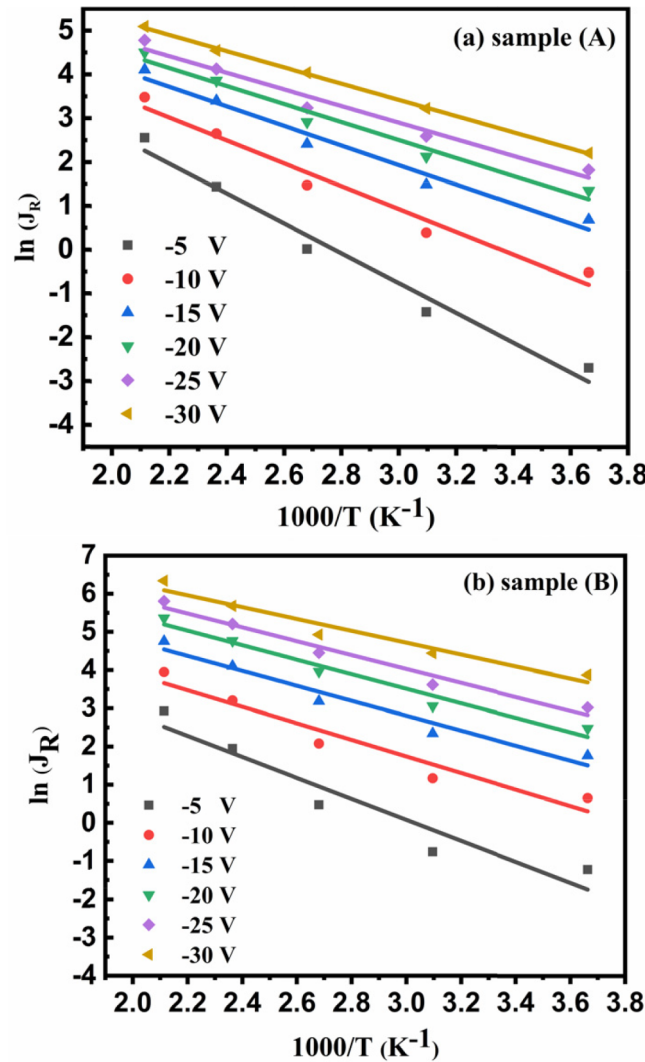


Fig. 8. $\ln (J_R)$ versus $1000/T$ plot of two samples at different gate bias.

E_a is the activation energy. The equation can be rearranged as

$$\ln(J_R) \propto -\frac{E_a}{K_B T} \quad (12)$$

As depicted in Fig. 8, it is clearly that the straight line can be fit well for the curve of $\ln (J_R)$ and $1000/T$ for the two samples at different gate bias. For the high reverse bias, the electrons are easy to obtain activation energy E_a and more possibility to emit into the trap states. Further, Fig. 9(a), (b) show the Arrhenius plot of $\ln (J_R)$ to extract the activation energy (E_a). At $V_R = -5$ V and $V_R = -25$ V, the values of E_a are 0.294 eV and 0.163 eV for sample (A), while 0.237 eV and 0.157 eV for sample (B), respectively. The extracted activation energy E_a at $V_R = -5$ V and $V_R = -25$ V are similar to that of 0.26 eV in [16] and 0.158 eV in [17], which indicates that thermally activated trap-assisted tunneling (TAT) is the dominant component of current at high reverse bias condition. In addition, E_a of sample (A) and sample (B) extracted under different bias are shown in Table 2. The extracted activation energy E_a of sample (A) is larger than the sample (B), which means the sample (B) is more prone to engender leakage than sample (A) at high reverse bias voltage. This results are consistent with the measured curve (J_R - V_R) as shown in Fig. 1 and Table 1. Moreover, for sample (A) and sample (B), the extracted E_a decrease as the reverse bias voltage increases as shown in Table 2. This mainly because the increase of the bias voltage will reduce the effective Schottky barrier height. Then the electron requires less amount of energy to tunnel through the barrier. In

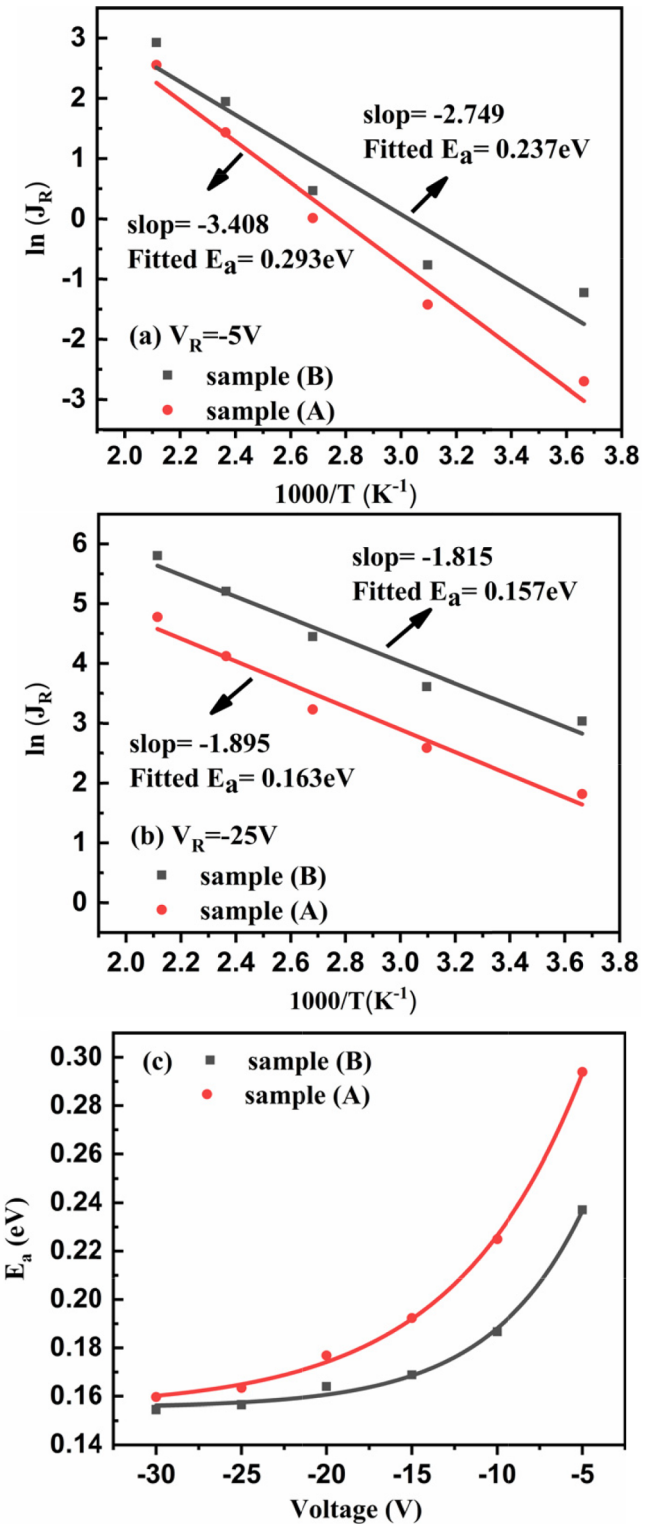


Fig. 9. (a), (b), $\ln (J_R)$ vs. $1000/T$ plot of two samples at $V_R = -5$ V and $V_R = -25$ V, respectively. And (c) E_a vs. V plot of sample (A) and sample (B), respectively.

order to analyze the trend of E_a with the reverse bias voltage, a fitting curve of E_a and reverse bias voltage is made as shown in Fig. 9(c). By analyzing the fitting results, exponential relationship can be found between E_a and the reverse bias voltage V_R , which can be describable as

Table 2

Extracting the activation energy of sample (a) and sample (b) at different bias.

Voltage (V)	Sample (A) Ea (eV)	Sample (B) Ea (eV)
-5	0.294	0.237
-10	0.225	0.187
-15	0.192	0.169
-20	0.177	0.164
-25	0.163	0.157
-30	0.160	0.155

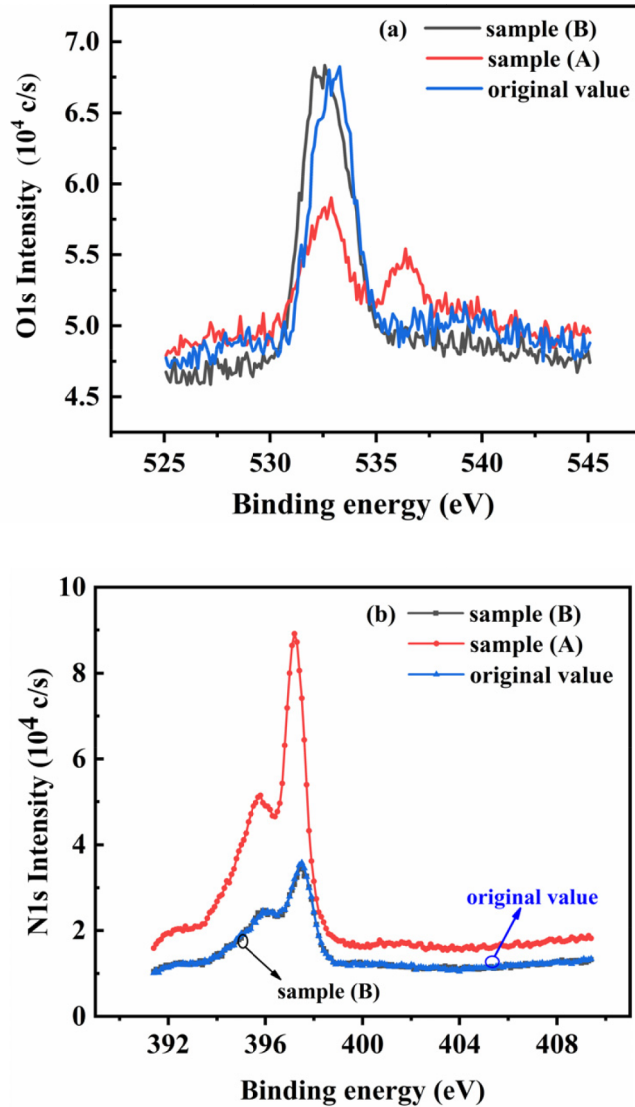


Fig. 10. XPS spectra of O1s and N1s levels of two samples.

$$E_a = A \exp\left(-\frac{V_R}{B}\right) + C \quad (13)$$

where A , B and C are related fitting parameters. The fitting parameters A , B and C are 0.268, -7.562 and 0.155 for sample (A), while 0.202 , -5.495 and 0.155 for sample (B), respectively. It is interesting that the fitting parameters C of the two samples are nearly the same at $V_R = -30$ V, which means the contribution of temperature to reverse leakage current of the two samples are the same at high reverse bias condition. Therefore, according to the TAT theory, the contribution of temperature to gate leakage of the two samples are the same. However, the leakage current of sample (B) is larger than that of sample (A), as

shown in Fig. 1. This is caused by the different trap states level, $q\varphi_t$, of the two samples as described in section A.

To further investigate the effect of the N_2 plasma surface treatment, x-ray photoelectron spectroscopy (XPS) measurements were performed on the gate recess area for the two samples before the gate mate formation. As shown in Fig. 10, the oxygen intensity of sample (A) has shrunk from 6.7×10^4 c/s to 5.7×10^4 c/s after the N_2 plasma surface treatment. While that of sample (B) remains the same. In addition, the concentration of N atoms increase a lot after the N_2 plasma surface treatment. The rate of N/O for the sample (A) and sample (B) with N_2 plasma surface treatment were 1.55:1 and 0.47:1, respectively. These results indicate that during the N_2 plasma surface treatment, the N atoms might replace the oxygen to recover related acceptor states, leading to the rise of trap levels and in turn decrease the gate leakage current. Therefore, the $q\varphi_t$ of sample (B) should be larger than that of sample (A), which is in good agreement with the calculated results as demonstrated above. Hashizume et al have also reported the N_2 plasma can effectively change the GaN surface Fermi level [18].

About the second peak at 536 eV, there may be some high bond energy oxides. P. D. Schulze et al has [19] reported that the second peak may be caused by H_2O near 536 eV.

Through the above analysis, the reverse gate leakage of both sample (A) and sample (B) in the high gate bias range are in accordance with the thermally activated TAT mechanism. However, as shown in Fig. 1, the leakage current density of the two samples actually increases slowly with the increase of reverse bias voltage (in region I, $V_R < V_{Th}$). And the Eq. (10) illustrates the reverse leakage current should be saturated with the increase of V_R . Considering that when $V_R < V_{Th}$, qn_{2DEG} is negligibly smaller compared with $q\sigma_p$, the electric field across the barrier layer, E , remains constant, as shown in Fig. 2. Further increase in reverse bias V_R is primarily dropped across the bulk GaN. Compare the epitaxial layer on SiC and sapphire substrate, large lattice mismatch exist between epitaxial GaN and Si (1 1 1) substrate, more defects are created in the GaN buffer layer ($\sim 5 \times 10^9 \text{ cm}^{-2}$ [17]). While the defects densities are about $8.2 \times 10^8 \text{ cm}^{-2}$ [20] and $1.0 \times 10^8 \text{ cm}^{-2}$ [21] on sapphire and SiC substrate. The defects in the depletion buffer layer may participate in the conduction under high bias condition. Therefore, considering these defects in buffer layer under high reverse gate voltage, the electric field in the barrier layer can be rearranged as,

$$E = \frac{q(\sigma_p - n_{2DEG})}{\varepsilon_0 \varepsilon_r} + \frac{qN_{it}}{\varepsilon_0 \varepsilon_{GaN}} \text{ For } V_R < < V_{Th} \quad (14)$$

where E is the electric field across the barrier, N_{it} is the defect density in the buffer layer, $\varepsilon_{GaN} = 9.0$ is the dielectric constant of GaN (buffer layer). Eq. (14) illustrate the electric field increases as defect density N_{it} increases. This further indicates that defect density N_{it} is more likely to affect the reverse leakage current under the high bias region. S. J. Rosner et al also reported that the defect density might participate in the conduction [9]. Therefore, this high density defects cause the

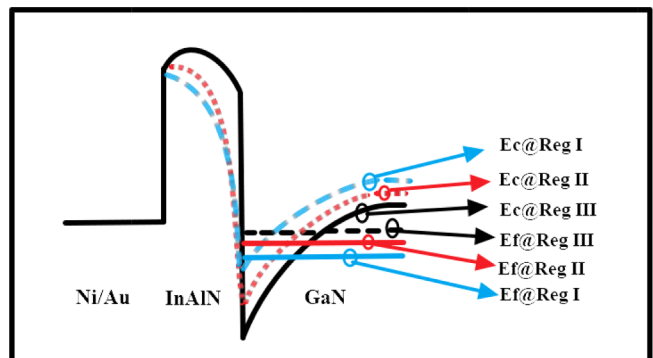


Fig. 11. Schematic band diagrams of InAlN/GaN HEMTs structures under the different regions.

reverse leakage increasing slowly with the increase of the electric field.

Through the above analysis, TAT is proved to be the dominant mechanism of reverse leakage current in ultrathin InAlN/GaN on Si (1 1 1) under different reverse bias voltages. The schematic band diagrams under the different reverse voltages have been drawn, as shown in Fig. 11. Compared to Reg III, the conduction band starts to bend as the electric field increases, the electrons tunnel through the trapezoidal barrier. When the electric field exceeds 4.97 MV/cm, the electrons tunnel through the triangular barrier in Reg II. And as the reverse bias is further increased, the depletion layer expands to the buffer layer. Due to the high density defects of Si based GaN buffer layer, the reverse leakage current further slowly increases with the reverse bias voltage in Reg I.

4. conclusion

In this paper, the transport mechanism of reverse leakage current for ultrathin InAlN/GaN HEMTs on 4 in Si (1 1 1) substrate is studied. The high-internal electric field in both of the samples with and without N₂ plasma surface treatment result in a large leakage current due to electron tunnelling through a thin Schottky barrier. Analysis based on common leakage mechanisms, for a wide range of reverse bias region ($-30 \text{ V} < V_R < 0 \text{ V}$) and temperature (237 K–473 K), the dominant leakage current of the two samples is proved to be TAT mechanism. The extracted trap states energy levels $q\phi_t$ with and without surface treatment are 1.37–1.42 eV and 1.2–1.60 eV at low reverse bias condition, while 2.7–3.5 eV and 2.4–4.55 eV at middle reverse bias, and the activation energy E_a are 0.160–0.294 eV and 0.155–0.237 eV at high reverse bias condition, respectively. These extracted values of trap energy levels and thermal activation energy together with the XPS data prove that the N₂ plasma surface treatment of the gate recess area of the InAlN/GaN HEMTs can effectively reduce the reverse gate leakage. Finally, a modified electric field model, which considering the influence of defects in the Si (1 1 1) based GaN buffer layer, is found to accurately explain the slow increment of the reverse bias leakage current under high reverse bias.

References

- [1] Kuzmik J, Pozzovivo G, Abermann S, Carlin JF, Gonschorek M, Feltin E, et al. Technology and performance of InAlN/AlN/GaN HEMTs with gate insulation and current collapse suppression using ZrO₂ or HfO₂. *IEEE Trans Electron Devices* 2008;55:937–41.
- [2] Zhou C, Jiang Q, Huang S, Chen KJ. Vertical leakage/breakdown mechanisms in AlGaN/GaN-on-Si devices. *IEEE Electron Device Lett* 2012;33:1132–4.
- [3] Medjdoub F, Alomari M, Carlin J-F, Gonschorek M, Feltin E, Py MA, Grandjean N, Kohn E. Thermal stability of 5 nm barrier in InAlN/GaN HEMTs. *Proc. ISDRS*. 2007. p. 1–2.
- [4] Turuvekere S, Karumuri N, Rahman AA, Bhattacharya A, DasGupta A, DasGupta N. Gate leakage mechanisms in AlGaN/GaN and AlInN/GaN HEMTs: comparison and modeling. *IEEE Trans Electron Devices* 2013;60:3157–65.
- [5] Ganguly Satyaki, Konar Aniruddha, Zongyang Hu, Xing Huili, Jena Debdeep. Polarization effects on gate leakage in InAlN/AlN/GaN high-electron-mobility transistors. *Appl Phys Lett* 2012;101. 253519-1-253519-5.
- [6] Kotani Junji, Yamada Atsushi, Ishiguro Tetsuro, Tomabechi Shuichi, Nakamura Norikazu. Low dislocation density InAlN/AlN/GaN heterostructures grown on GaN substrates and the effects on gate leakage characteristics. *Appl Phys Lett* 2016;108. 152109-1-152109-4.
- [7] Li Y, Ng GI, Arulkumaran S, Ye G, Liu ZH, Ranjan K, Ang KS. Investigation of gate leakage current mechanism in AlGaN/GaN high-electron-mobility transistors with sputtered TiN. *J Appl Phys* 2017;121. 044504-1-044504-7.
- [8] Arslan Engin, Buttin Serkan, Ozbay Ekmen. Leakage current by Frenkel-Poole emission in Ni/Au Schottky contacts on Al_{0.83}In_{0.17}N/AlN/GaN heterostructures. *Appl Phys Lett* 2009;94. 142106-1-142106-3.
- [9] Rosner SJ, Carr EC, Ludowise MJ, Girolami G, Erikson HI. Correlation of cathodoluminescence inhomogeneity with microstructural Defects in epitaxial GaN grown by metalorganic chemical-vapor deposition. *Appl Phys Lett* 1996;70:420–2.
- [10] Yan Dawei, Hai Lu, Cao Dongsheng, Chen Dunjun, Zhang Rong, Zheng Youdou. On the reverse gate leakage current of AlGaN/GaN high electron mobility transistors. *Appl Phys Lett* 2010;97. 153503-1-153503-1.
- [11] Liu ZH, Ng GI, Arulkumaran S, Maung YKT, Zhou H. Temperature-dependent forward gate current transport in atomic-layer-deposited Al₂O₃/AlGaN/GaN metal-insulator-semiconductor high electron mobility transistor. *Appl Phys Lett* 2011;98. 163501-1-163503-3.
- [12] Mahaveer Sathaiya D, Karmalkar Shreepad. Thermionic trap-assisted tunneling model and its application to leakage current in nitrided oxides and AlGaN/GaN high electron mobility transistors. *J Appl Phys* 2006;99. 093701-1-093701-6.
- [13] Liu Hui, Zhang Zongjing, Luo Weijun. Analysis of reverse gate leakage mechanism of AlGaN/GaN HEMTs with N₂ plasma surface treatment. *Solid-State Electroics* 2018;144:60–6.
- [14] Suzuki E, Schroder DK, Hayashi Y. Carrier conduction in ultrathin nitrided oxide films. *J Appl Phys* 1986;60:3616–21.
- [15] Lee Ji-Myon, Chang Ki-Myung, Kim Sa-Woo, Huh Chul, Lee In-Hwan, Seo-Ju Park. Dry etch damage in n-type GaN and its recovery by treatment with an N₂ plasma. *J Appl Phys* 2000;87:7667–70.
- [16] Liu ZH, Ng GI, Zhou H, Arulkumaran S, Maung YKT. Reduced surface leakage current and trapping effects in AlGaN/GaN high electron mobility transistors on silicon with SiN/Al₂O₃ passivation. *Appl Phys Lett* 2011;98. 113506-1-113506-3.
- [17] Miller EJ, Yu ET, Walterreit P, Speck JS. Analysis of reverse-bias leakage current mechanism in GaN grown by molecular-beam epitaxy. *Appl Phys Lett* 2004;84:535–7.
- [18] Hashizume Tamotsu, Ootomo Shinya, Oyama Susumu, Konishi Masanobu, Hasegawa Hideki. Chemistry and electric properties of surfaces of GaN and GaN/AlGaN heterostructures. *J Vac Sci Technol B* 2001;19:1675–81.
- [19] Schulze PD, Shaffer SL, Hance RL, Utley DL. Adsorption of water on rhenium studied by XPS. *J Vac Sci Technol A* 1983;1(1):97–9.
- [20] Andrew D. Koehler, Travis J. Anderson, Jennifer K. Hite, Bradley D. Weaver, Marko J. Tadjer, Michael A. Mastro, Jordan D. Greenlee, Petra Specht, Matthew Porter, Todd R. Weatherford, Karl D. Hobart, Fritz J. Kub, "Degradation mechanisms of AlGaN/GaN HEMTs on sapphire, Si, and SiC substrates under proton irradiation," 2014 IEEE Workshop on Wide Bandgap Power Devices and Applications., Knoxville, TN, USA, 33–35, 2014.
- [21] Leszczynski M, Prystawko P, Kruszewski P, Plesiewicz J, Kasalynas I, Dwiliński R, Zająć M, Kucharski R. Comparison of SiC and GaN Substrates Used for Epitaxy of HEMT Structures. *2013 European Microwave Conference*. 2003. p. 526–9.



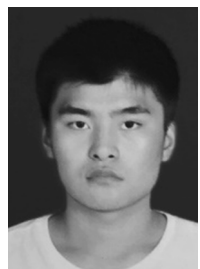
Jingxian Liang received the B.S. degrees in applied physics from North China University of Technology, in 2017. And he is now a M.S. candidate in Integrated Circuit Engineering from North China University of Technology, Beijing, China. Meanwhile, studying at Institute of Microelectronics of Chinese Academy of Sciences, Beijing, China. His research interests include GaN based microwave switching circuit and devices, particularly in X- and Ku-band.



Jie Zhang received the B.S. degree in microelectronics from North China University of Technology, Beijing, China, 2016. He is currently pursuing the M.S. degree in microelectronics with the Institute of Microelectronics, Chinese Academy of Sciences, Beijing, China. His current research interests include the design of microwave integrated circuit and the design of CMOS integrated circuit.



Ms. Jing Zhang is an Associate Professor at Microelectronics Department of North China University of Technology (NCUT). She got her Master Degree of Physics from Lanzhou University. Her research work is on low-k thin films, SiC power device, and integrated circuit testing. She has done a lot of work about the characteristics measurement of the semiconductor devices.



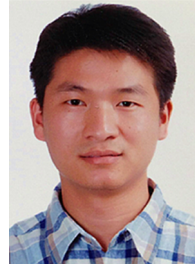
Longkun Lai received the B.S degree in microelectronics from Jiangnan University, Jiangsu, China, in 2017. He is now a M.S. candidate in microelectronics from Institute of Microelectronics of Chinese Academy of Sciences, Beijing, China. His research interests include design of Microwave integrated circuit and GaN level control circuit.



Xinyu Liu received the B.S. degree in physics from Anhui Normal University, Wuhu, China, in 1991, and the Ph.D. degree from the Institute of Microelectronics, Chinese Academy of Sciences, Beijing, China, in 1998. Since 1988, he has been involved in the GaAs- and GaN-based devices and monolithic microwave integrated circuits. He is currently a Vice Director of the Institute of Microelectronics.



Jin Xu received the B.S.degree from ChongqingUniversity, Chongqing, China, in 2017. He is currently pursuing the M.S.degree in microelectronics from the Institute of Microelectronics,Chinese Academy of Sciences, Beijing,China.His current research include the design of CMOS microwave integrated circuit, particularly in X-band.



Weijun Luo received the B.S. degree in Physics from Beijing Normal University, Beijing, China in 2003, and the Ph. D. degree in Institute of Semiconductors, Chinese Academy of Sciences in 2008. He joined Institute of Microelectronics, Chinese Academy of Sciences in 2008. Since then, he has been engaged in the GaN based devices and MMICs, including amplifier, phase shifter, switch, attenuator.